Journal of Inorganic and General Chemistry
ZAAC
Zeitschrift für anorganische und allgemeine Chemie
www.zaac.wiley-vch.de
RESEARCH ARTICLE

DOI: 10.1002/zaac.202400094

Nominal $CaAl_2Pt_2$ and Ca_2Al_3Pt – two new Intermetallic Compounds in the Ternary System Ca–Al–Pt

Stefan Engel,[a] Marcus Koch,[b] and Oliver Janka*[a]

Dedicated to Professor Michael Veith on the Occasion of his 80th Birthday

Single crystals of $CaAl_2Pt_2$, Ca_2Al_3Pt and Ca_2AlPt_2 were initially observed in an attempt to synthesize $Ca_3Al_4Pt_4$. Their structures were determined using single-crystal X-ray diffraction experiments. While nominal $CaAl_2Pt_2$ ($CaBe_2Ge_2$ type, *P4/nmm*, a = 426.79(2), c = 988.79(6) pm, wR_2 = 0.0679, 246 F^2 values and 18 variables) and Ca_2Al_3Pt (Mg_2Cu_3Si type, *P6$_3$/mmc*, a = 561.46(5), c = 876.94(8) pm, wR_2 = 0.0664, 214 F^2 values and 13 variables) exhibit Al/Pt mixing, for Ca_2AlPt_2 (Ca_2Ir_2Si type, *C2/c*, a = 981.03(2) b = 573.74(1), c = 772.95(2) pm, β = 101.862(1)° wR_2 = 0.0307, 2246 F^2 values and 25 variables) no mixing was observed. Subsequently, the nominal compositions were targeted with synthetic attempts from the elements using arc-melting and annealing techniques. For $CaAl_2Pt_2$ and Ca_2Al_3Pt always multi-phase mixtures were observed while Ca_2AlPt_2 could be obtained as almost X-ray pure material. Quantum-chemical calculations were used to investigate the charge transfer in these compounds rendering them polar intermetallics with a designated $[Al_xPt_y]^{\delta-}$ polyanion and $Ca^{\delta+}$ cations in the cavities of the polyanions.

1. Introduction

Ternary intermetallic compounds containing an alkaline earth element along with an electronegative transition metal (e.g. Ir, Pt, Au) and aluminum have been studied quite vigorously in the last decade. In contrast to most of their rare-earth containing counterparts (exceptions are Sc, Y, La and Lu), they exhibit no localized unpaired *f*-electrons which enables for example NMR spectroscopic studies[1,2] and simplifies quantum-chemical calculations for bonding and charge distribution analysis. A drawback, however, are the significantly different sizes of the Ca, Sr or Ba atoms (174, 192, 198 pm) or cations (106, 127, 143 pm)[3] which dramatically influence the existence of certain compositions and their respective crystal chemistry. Only a few isostructural series are known in the ternary *AE*–Al–Pt system, e.g. the orthorhombic $MgCuAl_2$ type compounds $AEAl_2Pt$ with *AE*=Ca, Sr and Ba[4] while the majority of compounds reported in the Pearson database[5] are singular (structural) entries. Examples are monoclinic Ca_2AlPt_2 (Ca_2Ir_2Si type, *C2/c*),[6] hexagonal $SrAl_2Pt_3$ ($CeCo_3B_2$ type, *P6/mmm*)[7] and $Ba_6Al_{53}Pt_{22}$ (own type, *P6$_3$/mcm*),[8] tetragonal $Sr_2Al_8Pt_3$ (anti-$Eu_2Ni_8Si_3$ type, *P4$_2$/nmc*),[9] modulated $SrAl_2Pt_2$[10] and $Ca_2Al_{15}Pt_6$[11] or orthorhombic CaAlPt (TiNiSi type, *Pnma*),[12,13] $Ca_2Al_9Pt_3$ ($Y_2Co_3Ga_9$ type, *Cmcm*),[14] $CaAl_5Pt_3$ (YNi_5Si_3 type, *Pnma*),[15] $SrAl_5Pt_3$ (YNi_5Si_3 type, *Pnma*),[16] $Ca_2Al_{16}Pt_9$ ($Ce_2Al_{16}Pt_9$ type, *Immm*),[17] $Sr_2Al_{16}Pt_9$ ($Ce_2Al_{16}Pt_9$ type, *Immm*)[16] and finally $Ba_3Al_4Pt_4$ (own type, *Cmcm*).[18]

Synthesizing isostructural compounds of the different alkaline earth elements is, as mentioned before, challenging due to the different atomic sizes. Easier, however, is the preparation of the Ca/Yb and Sr/Eu pairs. Here, for example, $EuAl_2Pt$[4] and $YbAl_2Pt$[19] in analogy to $SrAl_2Pt$ and $CaAl_2Pt$ could be obtained and $EuAl_5Pt_3$[20] as well as $Eu_2Al_{16}Pt_9$[17] were reported besides the Sr compounds. Furthermore, it was shown that $Yb_2Al_{15}Pt_6$[21] is isostructural to the Ca representative; interestingly, also the europium compound is known[22] while the strontium representative has not been reported thus far.

During attempts to synthesize $Ca_3Al_4Pt_4$ in analogy to $Ba_3Al_4Pt_4$, two new compounds were observed and characterized by means of single crystal X-ray diffraction experiments. $CaAl_2Pt_2$, which adopts the tetragonal $CaBe_2Ge_2$ type structure (*P4/nmm*) and Ca_2Al_3Pt, which crystallizes in the hexagonal Mg_2Cu_3Si type (*P6$_3$/mmc*). Furthermore, the initial reaction mixture contained single crystals of the already reported Ca_2AlPt_2 (Ca_2Ir_2Si type, *C2/c*). We report on the structural investigations on these three compounds, on the attempts to obtain phase pure bulk samples and the analysis of the charge transfer using quantum-chemical calculations.

[a] *S. Engel, O. Janka*
Saarlandes University, Solid State Inorganic Chemistry, Campus C4 1, 66123 Saarbrücken, Germany
E-mail: oliver.janka@uni-saarland.de
[b] *M. Koch*
INM-Leibniz Institute for New Materials, Campus D2 2, 66123, Saarbrücken, Germany

Supporting information for this article is available on the WWW under https://doi.org/10.1002/zaac.202400094

Experimental

Synthesis

Initially, $Ca_3Al_4Pt_4$ was prepared in analogy to $Ba_3Al_4Pt_4$,[18] subsequent syntheses were conducted on stoichiometry for Ca_2AlPt_2, $CaAl_2Pt_2$ and Ca_2Al_3Pt. All samples were prepared from the elements using calcium pieces (Onyxmet), platinum pieces (Agosi AG) and aluminum turnings (Onyxmet), all with stated purities above 99%. Samples were prepared on a 300 mg scale. The Ca pieces were stored in an argon filled drybox; surface contaminations on the pieces were removed mechanically prior to the reaction. For the reaction, the elements were arc-welded[23] in tantalum tubes in an argon atmosphere of about 800 mbar with the different molar ratios given above. The argon gas was purified over a titanium sponge (873 K), molecular sieves and silica gel prior to the use. The sealed tantalum ampoules were placed in the water-cooled sample chamber of an induction furnace (Trumpf Hüttinger, TruHeat HF 5010).[24] Water-cooling was used to prevent reactions of the Ta ampoules with the sample chamber. The Ta containers were heated to ~1500 K within 2 minutes, dwelled at that temperature for 10 min followed by slow cooling to ~1000 K. The cooling was achieved by reducing the power output of the generator, leading to a cooling rate of about 100 K min^{-1}. After an annealing step of 4 h at this temperature, the samples were cooled naturally by shutting off the power supply. All samples could easily be separated from the container material afterwards and no reactions with the tantalum ampoules could be observed. The samples were metallic, ground powders are grey.

Powder and Single Crystal X-ray Diffraction

The polycrystalline samples were analyzed by powder X-ray diffraction (PXRD) experiments. The PXRD patterns of the pulverized samples were recorded at room temperature on a D8-A25 Advance diffractometer (Bruker, Karlsruhe, Germany) in Bragg-Brentano θ–θ geometry (goniometer radius 280 mm) with non-monochromatized Cu$K\alpha$ radiation ($\lambda = 154.0596$ pm). A 12 µm Ni foil working as $K\beta$ filter and a variable divergence slit were mounted at the primary beam side. A LYNXEYE detector with 192 channels was used at the secondary beam side. Experiments were carried out in a 2θ range of 6 to 130° with a step size of 0.013° and a total scanning time of 1 h. The recorded data was evaluated using the Bruker TOPAS 5.0 software,[25] using the fundamental parameter approach and the Rietveld method.[26,27]

From the annealed crushed samples, single crystals of nominal Ca_2AlPt_2, $CaAl_2Pt_2$ and Ca_2Al_3Pt were isolated and investigated at room temperature on a Bruker X8 APEX2, Nonius κ-CCD diffractometer, operating with graphite monochromated MoKα (λ = 0.71073 Å) radiation. Multi-scan absorption corrections using the Bruker SadABS data package[28] were applied to the data sets. The data were solved and refined using SUPERFLIP[29] and JANA2006.[30–32] Details on the structure refinement, atomic coordinates as well as interatomic distances are compiled in Tables 1–4. Structural drawing were generated with Diamond 4[33] and edited with Adobe Illustrator CS6.

CSDs 2331503–2331505 contain the supplementary crystallographic data for this paper. The data can be obtained free of charge from The Cambridge Crystallographic Data Centre via www.ccdc.cam.ac.uk/structures.

Energy-Dispersive X-ray Spectroscopy (EDX)

The single crystals of nominal Ca_2AlPt_2, $CaAl_2Pt_2$ and Ca_2Al_3Pt, investigated on the diffractometer, were semiquantitatively analyzed on an SEM FEI Quanta 400 (FEI, Hilsboro, United States) scanning electron microscope equipped with an EDAX Genesis V6.04 EDX detector (EDAX, Unterschleissheim, Germany) using CaO, Pt and Al_2O_3 as standards. The point measurements on the surfaces of all three crystals clearly showed that all three elements are present, and no tantalum (container material) could be observed. However, the deviations from the weighed and refined compositions are quite significant which can be explained by the irregular crystallite faces, the not perfect perpendicular orientation of the crystal towards the beam and coverage of beeswax on the crystal surface. This leads to a significantly decreased amount of Al in the EDX spectra measured.

Quantum-Chemical Calculations

Electronic structure calculations of nominal Ca_2AlPt_2, $CaAl_2Pt_2$ and Ca_2Al_3Pt were performed using the projector augmented wave method (PAW) of Blöchl[34,35] coded in the Vienna ab initio simulation package (VASP).[36,37] VASP calculations employed the potentials PAW_PBE Ca_sv 06Sep2000, PAW_PBE Pt_pv 12Dec2005 and PAW_PBE Al 04Jan2001. The cutoff energy for the plane wave calculations was set to 800 eV and the Brillouin zone integration was carried out using a *k*-point mesh with a spacing of ≈0.02 for all compounds.

Table 1. Lattice parameters and unit cell volumes of Ca_2AlPt_2 (*C*2/*c*, *Z* = 4, Ca_2Ir_2Si type), $CaAl_2Pt_2$ (*P*4/*nmm*, *Z* = 2, $CaBe_2Ge_2$ type) and Ca_2Al_3Pt (*P*6$_3$/*mmc*, *Z* = 2, Mg_2Cu_3Si type) determined by powder X-ray diffraction and single crystal diffraction.

Compound	*a* (pm)	*b* (pm)	*c* (pm)	*β* (°)	*V* (nm^3)
Ca_2AlPt_2					
Single crystal	981.03(2)	573.74(1)	772.95(2)	101.862(1)	0.4258
Powder	981.0(1)	573.8(1)	772.9(1)	101.847(1)	0.4258
DFT	977.9	568.7	770.2	102.11	0.4183
$CaAl_2Pt_2$					
Single crystal	426.79(2)	*a*	988.79(6)	90	0.1801
Powder	423.6(1)	*a*	963.5(1)	90	0.1729
DFT	412.2	*a*	1074.3	90	0.1825
Ca_2Al_3Pt					
Single crystal	561.46(5)	*a*	876.94(8)	90	0.2394
Powder	561.7(1)	*a*	876.8(1)	90	0.2396
DFT	556.6	*a*	869.3	90	0.2332

Table 2. Crystallographic data and structure refinement for nominal Ca_2AlPt_2 (*C*2/*c*, *Z* = 4, Ca_2Ir_2Si type), $CaAl_2Pt_2$ (*P*4/*nmm*, *Z* = 2, $CaBe_2Ge_2$ type) and nominal Ca_2Al_3Pt (*P*6$_3$/*mmc*, *Z* = 2, Mg_2Cu_3Si type).

Nominal composition	Ca_2AlPt_2	$CaAl_2Pt_2$	Ca_2Al_3Pt
Refined composition	Ca_2AlPt_2	$CaAl_{2.24(1)}Pt_{1.76(1)}$	$Ca_2Al_{3.09(1)}Pt_{0.91(1)}$
CCDC number	2331504	2331503	2331505
Lattice parameters		see Table 1	
Molar mass, g mol^{-1}	497.3	443.9	341.1
Density calc., g cm^{-3}	7.76	8.18	4.73
Crystal size, µm	55×45×30	40×25×20	45×35×30
Detector distance, mm	40	40	40
Exposure time, s	20	20	20
Range in *hkl*	−21, +20; ±12; ±16	±6; +6,−5; +15,−10	±8; ±8; ±13
θ_{min}, θ_{max}, deg	4.14-50.09	4.12-33.15	4.19-33.74
Linear absorption coeff., mm^{-1}	68.0	70.0	29.2
No. of reflections	27558	2449	4761
R_{int}/R_σ	0.0368/0.0157	0.0431/0.0257	0.0315/0.0113
No. of independent reflections	2246	246	214
Reflections used [$I \geq 3\sigma(I)$]	2198	222	206
F(000), e	836	378	303
R_1/wR_2 for $I \geq 3\ \sigma(I)$	0.0164/0.0304	0.0274/0.0671	0.0193/0.0659
R_1/wR_2 for all data	0.0170/0.0307	0.0313/0.0679	0.0204/0.0664
Data/parameters	2246/25	246/18	214/13
Goodness-of-fit on F^2	2.07	1.85	2.59
Extinction coefficient	340(20)	21(16)	430(70)
Diff. Fourier residues/e$^-$ Å^{-3}	+3.38/−1.71	+3.10/−2.97	+2.61/−0.66

Table 3. Atom positions and equivalent isotropic displacement parameters (pm^2) for Ca_2AlPt_2 (*C*2/*c*, *Z* = 4, Ca_2Ir_2Si type), nominal $CaAl_2Pt_2$ (*P*4/*nmm*, *Z* = 2, $CaBe_2Ge_2$ type) and nominal Ca_2Al_3Pt (*P*6$_3$/*mmc*, *Z* = 2, Mg_2Cu_3Si type). U_{eq} is defined as one third of the trace of the orthogonalized U_{ij} tensor.

Atom	Wyckoff Position	*x*	*y*	*z*	U_{eq} (pm^2)	site occ.
Ca_2AlPt_2						
Ca	8*f*	0.64998(5)	0.63116(7)	0.14872(7)	71(1)	1
Pt	8*f*	0.87101(1)	0.63388(1)	0.49584(1)	47(1)	1
Al	4*e*	0	0.3927(2)	3/4	60(2)	1
$CaAl_{2.24(1)}Pt_{1.76(1)}$						
Ca	2*c*	1/4	1/4	0.7562(3)	142(7)	1
Pt1	2*a*	3/4	1/4	0	120(2)	0.80(1)
Al1′	2*a*	3/4	1/4	0	120(2)	0.20(1)
Pt2	2*c*	1/4	1/4	0.3560(14)	101(9)	0.69(5)
Pt2′	2*c*	1/4	1/4	0.3814(10)	101(9)	0.31(5)
Al1	2*b*	3/4	1/4	1/2	125(11)	1
Al2	2*c*	1/4	1/4	0.1109(10)	170(20)	1
$Ca_2Al_{3.09(1)}Pt_{0.91(1)}$						
Ca	4*f*	2/3	1/3	0.0571(1)	80(4)	1
Pt1	2*a*	0	0	0	66(2)	0.90(1)
Al1	2*a*	0	0	0	66(2)	0.10(1)
Pt2	6*h*	0.1629(1)	2*x*	1/4	75(6)	0.01(1)
Al2	6*h*	0.1629(1)	2*x*	1/4	75(6)	0.99(1)

The calculations are done starting from the experimental crystal data and the whole cell undergoes unconstrained geometry relaxing of the structure parameters and coordinates. At high precision integration of the Brillouin-zone (BZ) (Ca_2AlPt_2: 9×15×11; $CaAl_2Pt_2$: 15×15×9; Ca_2Al_3Pt: 13×13×9) the charge density issued from the accurate calculations was analyzed using the AIM (atoms in molecules theory) approach[38] developed by Bader who devised an intuitive way of splitting molecules into atoms as based purely on the electronic charge density. The charge density reaches a minimum between atoms defining thus a region separating atoms from each other. In the case of a family of compounds such an analysis can be useful to establish trends. Core electrons are included for an accurate account of the charge density. The analysis is done using a fast algorithm operating on a charge density grid. The obtained charges are listed in Table 5.

Table 4. Interatomic distances (pm) for Ca_2AlPt_2 (*C*2/*c*, $Z=4$, Ca_2Ir_2Si type), nominal $CaAl_2Pt_2$ (*P*4/*nmm*, $Z=2$, $CaBe_2Ge_2$ type) and nominal Ca_2Al_3Pt (*P*6$_3$/*mmc*, $Z=2$, Mg_2Cu_3Si type). All distances of the first coordination spheres are listed. All standard uncertainties were less than 0.2 pm.

Ca_2AlPt_2											
Ca	1	Pt	305.6	Al	2	Pt	249.5	Pt	1	Al	249.5
	1	Pt	306.2		2	Pt	252.1		1	Al	252.0
	1	Pt	307.6						1	Pt	273.5
	2	Pt	308.4						1	Pt	295.0
	1	Pt	310.5								
	1	Al	327.3								
	1	Al	336.4								
	1	Al	347.1								
$CaAl_2Pt_2$											
Ca	4	Pt2	321.5	Al1	4	Pt2′	243.5	Pt1/Al1′	4	Al2	239.9
	4	Pt1/Al1′	321.9		4	Pt2	256.5		4	Pt1/Al1′	301.8
	4	Al2	329.2		4	Al1	301.8				
	4	Pt2′	331.1					Pt2	1	Pt2′	25.1
	4	Al1	331.3	Al2	4	Pt1/Al1	239.9		1	Al2	242.2
					1	Pt2′	267.5		4	Al1	256.5
					1	Pt2	242.4				
								Pt2′	1	Pt2	25.1
									4	Al1	256.5
									1	Al2	242.2
Ca_2Al_3Pt											
Ca	3	Al2/Pt2	316.3	Pt1/Al1	6	Pt2/Al2	270.5	Pt2/Al2	2	Pt1/Al1	270.5
	6	Al2/Pt2	327.8						2	Pt2/Al2	274.3
	3	Pt1/Al1	328.0						2	Pt2/Al2	287.1
	1	Ca	338.3								
	3	Ca	339.3								

Table 5. Bader charges considering valence states.

	Ca	Al	Pt	Ref.
Ca_2AlPt_2	+1.30	+1.30	−1.95	*
Ca_2AlPt_2	+1.10	+0.62	−1.42	[6]
$CaAl_2Pt_2$	+1.36	+1.76/+1.74	−3.08/−1.76	*
Ca_2Al_3Pt	+1.20	+0.30	−3.30	*

* this work.

2. Results

2.1. Ternary System Ca–Al–Pt

The known phases in the ternary system Ca–Al–Pt are shown in Figure 1. A number of binary phases have been reported in the three systems Ca–Al, Ca–Pt and Al–Pt. A rule of thumb states, that in ternary systems where numerous binary phases are known, also numerous ternary phases should exist. Thus far, the equiatomic CaAlPt, $CaAl_2Pt$, Ca_2AlPt_2 and the Al-rich $Ca_2Al_9Pt_3$ have been reported. CaAlPt crystallizes in the orthorhombic TiNiSi type structure (*Pnma*),[12,13] while $CaAl_2Pt$ adopts the also orthorhombic $MgCuAl_2$ type structure (*Cmcm*)[4] and $Ca_2Al_9Pt_3$ crystalizes in the $Y_2Co_3Ga_9$ type (*Cmcm*).[14] Finally, monoclinic Ca_2AlPt_2 (*C*2/*c*, Ca_2Ir_2Si type) has also been reported.[6] During attempts to synthesize $Ca_3Al_4Pt_4$, tetragonal $CaAl_2Pt_2$ (*P*4/*nmm*, $CaBe_2Ge_2$ type) and hexagonal Ca_2Al_3Pt (*P*6$_3$/*mmc*, Mg_2Cu_3Si type) were discovered. In addition, Ca_2AlPt_2 was observed and subsequently resynthesized.

2.2. Powder X-ray Diffraction

A sample with a nominal starting composition of $Ca_3Al_4Pt_4$ was prepared, in analogy to $Ba_3Al_4Pt_4$,[18] from which single crystals of monoclinic Ca_2AlPt_2, tetragonal $CaAl_2Pt_2$ and hexagonal Ca_2Al_3Pt were extracted and investigated via single crystal X-ray diffraction experiments (*vide infra*). The powder X-ray diffraction pattern indicates the formation of a multi-phase mixture. Ca_2AlPt_2, $CaAl_2Pt_2$, Ca_2Al_3Pt as well as $CaAl_2Pt$ and in addition, at least one yet unidentified side phase, are present in the sample. Subsequently, new samples with the respective nominal compositions Ca_2AlPt_2, $CaAl_2Pt_2$ and Ca_2Al_3Pt were prepared. Ca_2AlPt_2 was obtained as nearly phase pure sample. The Rietveld refinement of the powder X-ray data is shown in Figure 2. The desired phase Ca_2AlPt_2 was obtained with 99(1) wt.–%, with an additional 1(1) wt.–% of cubic AlPt (*P*2$_1$3, FeSi type[39]). For $CaAl_2Pt_2$ and Ca_2Al_3Pt, no phase pure samples could be obtained. For the first, in addition to the targeted compound, also $AlPt_3$ and $Al_{21}Pt_8$ as well as a yet unidentified phase could be observed in the powder diffraction patterns. The samples of nominal Ca_2Al_3Pt indicate the formation of the desired phase as well as $CaAl_2Pt$ and an unknown compound. Attempts to identify the two unknown compounds in the

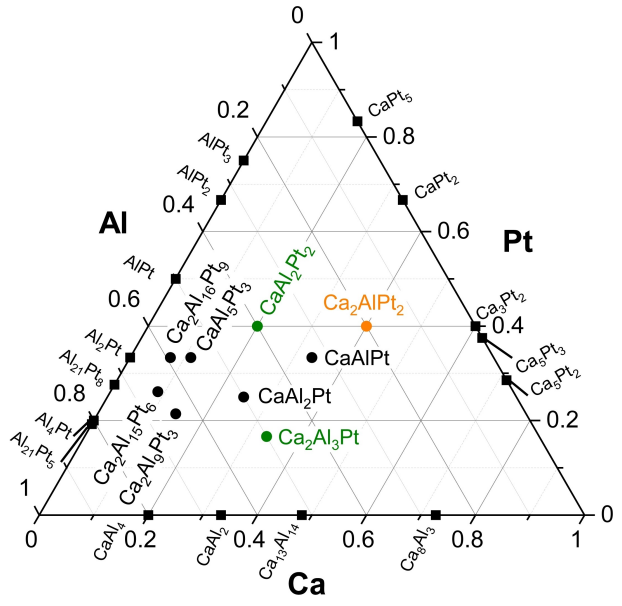

Figure 1. Overview of the binary and ternary phases known in the system Ca–Al–Pt. Data are taken from the Pearson database[5] and the references cited in the introduction. New reported phases are shown in green, the resynthesized phase in orange.

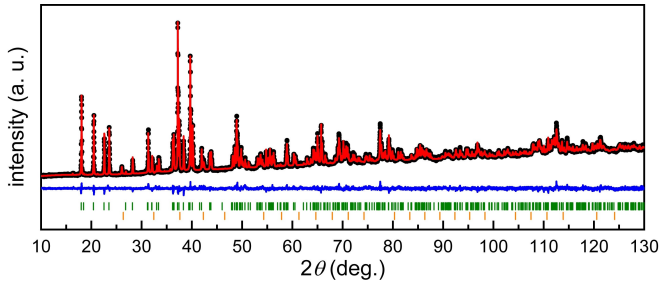

Figure 2. Rietveld refinement of the powder X-ray diffraction pattern of Ca_2AlPt_2. Collected data are shown as black dots, the refinement as red, the difference as blue line. Green ticks indicate the Bragg positions of Ca_2AlPt_2, orange ticks the ones of AlPt.

samples of nominal $CaAl_2Pt_2$ and Ca_2Al_3Pt via single-crystal X-ray diffraction experiments have not been successful thus far.

2.3. Single Crystal X-ray Diffraction and Structure Refinement

From the sample with the nominal composition $Ca_3Al_4Pt_4$, numerous single crystals were selected and analyzed. Careful analysis of the data of the first single crystal X-ray diffraction experiment revealed a *C*-centered monoclinic lattice and space group *C*2/*c* was found to be correct for Ca_2AlPt_2. The Ca_2Ir_2Si type structure could be assigned, in accordance to the report in literature.[6] For what turned out to be $CaAl_{2.24(1)}Pt_{1.76(1)}$, a tetragonal metric was observed and space group *P*4/*nmm* along with the $CaBe_2Ge_2$ type structure was deduced. Finally, $Ca_2Al_{3.09(1)}Pt_{0.91(1)}$ crystallizes in the hexagonal crystal system with space group $P6_3/mmc$ and adopts the Mg_2Cu_3Si type structure, a coloring variant of the hexagonal Laves phase $MgZn_2$.

All structures were solved using the charge flipping algorithm of Superflip[29] and least squares refinements on F^2 using the program Jana2006[30,31] were carried out. All atomic positions were refined with anisotropic displacement parameters and as a check for correct compositions, the occupancy parameters were refined in a separate series of least-square refinements.

While for Ca_2AlPt_2 no mixed occupancies were observed, nominal Ca_2Al_3Pt shows mixing of Pt and Al on the 2*a* and 6*h* site leading to a refined composition of $Ca_2Al_{3.09(1)}Pt_{0.91(1)}$. It has to be noted, that the mixing on the 6*h* site refines to 0.99(1) Al and 0.01(1) Pt, however, when refining solely as Al, this position refines to a site occupancy of 1.04(1), clearly indicating a mixing with Pt. Due to the significant differences in electron density between Al and Pt only around 1% Pt is refined on this site. Also, the *R*-values show that a mixing is appropriate since they decrease from 0.0213/0.0714 to 0.0204/0.0664 for R_1/wR_2 for all data.

Nominal $CaAl_2Pt_2$ exhibits Pt and Al mixing on the 2*a* site. In addition, significant residual electron density near the Pt2 position (2*c*) can be observed with a distance of ~66 pm. Therefore, this site has been refined as a split site with a constrained overall occupation of 1 and constrained displacement parameters but the possibility to freely refine the *z* parameter. This leads to a composition of $CaAl_{2.24(1)}Pt_{1.76(1)}$. The final difference Fourier syntheses for all three structures were contour less. Details of the structure determination, atomic parameters and interatomic distances can be found in Tables 1–4. CSDs 2331503–2331505 contains the supplementary crystallographic data for this paper. These data can be obtained free of charge from The Cambridge Crystallographic Data Centre via www.ccdc.cam.ac.uk/data_request/cif.

2.4. Crystal Chemistry

In the following paragraph, the three structure types will be briefly introduced, a detailed structure description, however, can be found in the respective original papers. The unit cells are depicted in Figure 3. We will begin with nominal $CaAl_2Pt_2$ which crystallizes in the tetragonal crystal system with space group *P*4/*nmm*, isostructural to $CaBe_2Ge_2$.[40] The structure can be derived from $BaAl_4$ via a *klassengleiche* transition of index 2 leading to a split of the two crystallographically independent Al sites in $BaAl_4$.[41–43] Therefore, five crystallographic atom positions (2*a*, 2*b* and 3×2*c*) can be found in the $CaBe_2Ge_2$ type.[40] The Ca position is also occupied by Ca atoms in nominal $CaAl_2Pt_2$, while the Al1 and Al2 atoms occupy the Be positions of the prototype. The Ge atoms of the prototype are finally replaced by Pt atoms. The refinement, however, indicates that Pt1 position in nominal $CaAl_2Pt_2$ is not fully occupied by Pt. A freely refined occupancy factor led to a reduced site occupation. Therefore, a mixed occupied site with Al was introduced (Figure 3, segmented black/white spheres) as this has been

Journal of Inorganic and General Chemistry
ZAAC
Zeitschrift für anorganische und allgemeine Chemie

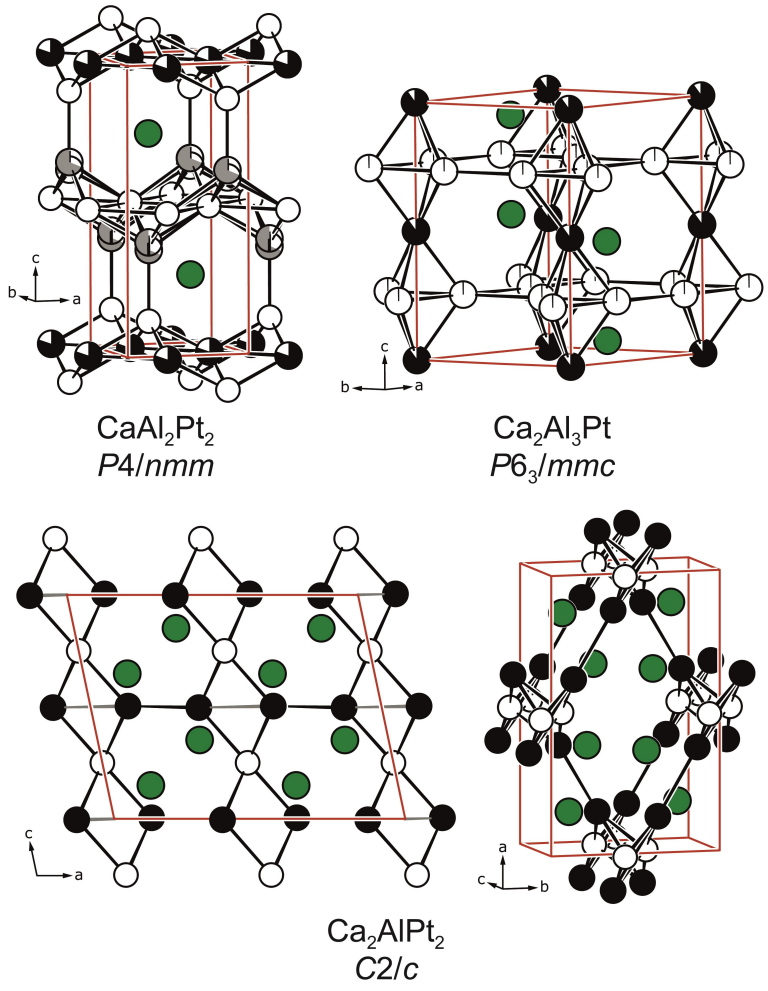

Figure 3. Unit cells of (*top left*) $CaAl_2Pt_2$ ($CaBe_2Ge_2$ type, *P*4/*nmm*) depicted roughly along the *b* axis; (*top right*) Ca_2Al_3Pt (Mg_2Cu_3Si type, *P*6$_3$/*mmc*) and (*bottom*) Ca_2AlPt_2 along the *b* and roughly along the *c* axis. Ca, Al and Pt atoms are shown in green, white and black circles. Partially occupied sites are shown as segmented or grey circles (see text).

observed in $BaAl_4$ related compounds.[44] The Pt2 position exhibits a significantly enhanced anisotropic displacement parameter as well as residual electron density nearby (*d* ~60 pm). A refinement of the occupancy parameter of the Pt2 site led to a significant improve in the *R*-values, however, the additional electron density did not vanish. Therefore, the Pt2 site was refined as a split position with both the ADPs and the overall composition fixed (Figure 3, grey spheres). This leads to a refined composition of $CaAl_{2.24(1)}Pt_{1.76(1)}$. It is interesting to note that $SrAl_2Pt_2$ also exists and crystallizes in a (3 + 2)D incommensurately modulated structure[10] related to the $CaBe_2Ge_2$ type. However, even upon close inspection, no superstructure reflections are visible for $CaAl_2Pt_2$. And also, the defects observed in modulated $SrPt_{1.833}\square_{0.167}Sn_2$ are not applicable here.[45] The interatomic distances in $CaAl_{2.24(1)}Pt_{1.76(1)}$ (*d*(Ca–Pt) = 322–331 pm; *d*(Ca–Al) = 329–351 pm; *d*(Al–Pt) = 240–268 pm; *d*-(Pt–Pt) = 302 pm; *d*(Al–Al) = 302 pm) are in agreement with other binaries like Al_2Pt (CaF_2 type, *d*(Al–Pt) = 256 pm; *d*(Al–Al) - = 296 pm),[46] $CaAl_2$ ($MgCu_2$ type, *d*(Al–Al) = 284 pm; *d*(Ca–Al) = 333 pm)[47] or $CaPt_2$ ($MgCu_2$ type, *d*(Pt–Pt) = 270 pm; *d*(Ca–Pt) = 316 pm)[48] or ternaries like CaAlPt (*d*(Ca–Pt) = 294–305 pm; *d*(Ca–Al) = 308–336 pm; *d*(Al–Pt) = 261–275 pm; *d*(Al–Al) = 311 pm),[12,13] $Ca_2Al_9Pt_3$ (*d*(Ca–Pt) = 343–347 pm; *d*(Ca–Al) = 303–318 pm; *d*(Al–Pt) = 257–264 pm; *d*(Al–Al) = 269–293 pm)[14] or $CaAl_2Pt$ (*d*(Ca–Pt) = 284–314 pm; *d*(Ca–Al) = 323–342 pm; *d*-(Al–Pt) = 255–258 pm; *d*(Al–Al) 276–290 = pm).[4] The relatively short Al–Pt distances point towards bonding interactions.

Nominal Ca_2Al_3Pt (Figure 3, *top right*) crystallizes in the hexagonal Mg_2Cu_3Si type, an ordering variant of the hexagonal Laves phase $MgZn_2$. Two structural reviews on Laves phases addressing the ordering variants have been published recently.[49,50] It is interesting to note, that the Al phases usually exhibit a M_2Al_3T composition (*M*=Sc, Y, La–Nd, Sm, Gd–Lu; *T*= Ru, Rh, Ir),[51,52] while the isostructural gallides have a M_2GaT_3 stoichiometry (*M*=Y, La–Nd, Sm, Gd–Er; *T*=Rh).[53] With the early transition metal Ti, the M_2Al_3Ti series (*M*=Y, Gd–Tm, Lu) adopts the rhombohedral Mg_2Ni_3Si type structure.[54] Since the Mg_2Ni_3Si type is a coloring variant of $MgZn_2$, the structure description is straightforward. The Zn1 site (6 *h*) is occupied by Al atoms while the Pt atoms reside on the Zn2 site (2*a*). The Ca atoms can be

finally found on the Mg position (4*f*) of the prototype. As for the rare-earth compounds RE_2Al_3T with *RE*=Sc, Y, La–Nd, Sm, Gd–Lu and *T*=Ru, Rh, Ir,[51] mixing of the Al and the transition metal atoms can take place. In nominal Ca_2Al_3Pt, nearly 10% Al can be found on the Pt site (2*a*) while 1% Pt can be observed on the Al site (6*h*). This leads to a refined composition of $Ca_2Al_{3.09(1)}Pt_{0.91(1)}$. The interatomic distances in $Ca_2Al_{3.09(1)}Pt_{0.91(1)}$ (*d*(Ca–Pt)=328 pm; *d*(Ca–Al)=316 & 328 pm; *d*(Al–Pt)=270 pm; *d*(Al–Al)=274 & 287 pm) are in agreement with the compounds named before. And again, the relatively short Al–Al and Al–Pt distances point towards bonding interactions.

Ca_2AlPt_2 (Figure 3, *bottom*) finally crystallizes in the monoclinic crystal system and adopts the Ca_2Ir_2Si type structure. In the crystal structure, the Pt atoms form chains with alternating distances (*d*(Pt–Pt)=274 & 295 pm) running within the *ab* plane. The Pt chains are found on *z*=0 and 1/2 with an angle of 61° to each other. The Al atoms connect these Pt chains forming cavities for the Ca atoms. The atomic arrangement is similar to the one observed in the Ca_2Pd_2Ge type structure,[6] however, the distinct difference are the alternating Pt–Pt distances in the chains. In contrast to the two structures mentioned before, no mixing of Al and Pt was observed. The interatomic distances in Ca_2AlPt_2 (*d*(Ca–Pt)=306-311 pm; *d*(Ca–Al)=327-351 pm; *d*(Al–Pt)=249-252 pm; *d*(Pt–Pt)=274 & 295 pm) are again in agreement with the compounds named in the discussion about nominal $CaAl_2Pt_2$. In contrast to the two structure types named before, no Al–Al bonding was observed.

2.5. Quantum-Chemical Calculations

Quantum-mechanical calculations were performed on the DFT level using the experimental lattice parameters and atomic positions as starting points. The idealized structures, with respect to mixed occupancies, were used. In the cases of Ca_2AlPt_2 and Ca_2Al_3Pt the unit cell parameters after structural relaxation are in good agreement with the experimentally observed lattice parameters. For $CaAl_2Pt_2$, however, significant deviations are observed. This can be probably related to the fact that the starting lattice parameters of ideal $CaAl_2Pt_2$ are in fact the ones of $CaAl_{2.24(1)}Pt_{1.76(1)}$ which exhibits severe mixing of Al and Pt, which was removed for the quantum-chemical calculations. After structural relaxation (Table 1), self-consistent runs were conducted and subsequent high precision integrations of the Brillouin-zone (BZ) (Ca_2AlPt_2: 9×15×11; $CaAl_2Pt_2$: 15×15×9; Ca_2Al_3Pt: 13×13×9) were used for the calculation of the Bader charges [21], the obtained Bader charges are listed in Table 5. It should be noted, that Doverbratt and coworkers already calculated Bader charges for Ca_2AlPt_2[6] which differ to the values reported in this work, most likely due to the use of different functionals. However, the overall trend is the same. When looking at the trends of the Bader charges, the Ca and Al atoms exhibit positive charges while the Pt atoms are formally anionic. This is in line with the Pauling electronegativities (χ(Ca)=1.00; χ(Al)=1.61; χ(Pt)=2.28) of the constituent elements. When going from Ca_2AlPt_2 (40 at.–% Ca; 40 at.–% Pt) over $CaAl_2Pt_2$ (20 at.–% Ca; 40 at.–% Pt) to Ca_2Al_3Pt (33.3 at.–% Ca; 16.7 at.–% Pt) the absolute values of the overall charge of the Pt atoms increases significantly from −1.42 to −3.30. This can also be easily explained by the fact that the Pt content decreases, hence the ratio of electronegative Pt to the less electronegative Ca and Al shifts, leading to an increased charge transfer. Overall, all three compounds should therefore be regarded as polar intermetallic compounds with Ca cations compensated by $[Al_xPt_y]^{\delta-}$ polyanions.

3. Conclusion

With tetragonal $CaAl_2Pt_2$ ($CaBe_2Ge_2$ type) and hexagonal Ca_2Al_3Pt ($MgZn_2/Mg_2Cu_3Si$ type), two new intermetallic compounds have been found in the ternary system Ca–Al–Pt upon attempts to synthesize $Ca_3Al_4Pt_4$, in analogy to $Ba_3Al_4Pt_4$. In addition, the already reported monoclinic Ca_2AlPt_2 (Ca_2Ir_2Si type) was observed. Single crystal X-ray diffraction experiments showed that the latter compound has a defined composition, while nominal $CaAl_2Pt_2$ and Ca_2Al_3Pt exhibit significant Al/Pt mixing. The refined compositions of the investigated single crystals are $CaAl_{2.24(1)}Pt_{1.76(1)}$ and $Ca_2Al_{3.09(1)}Pt_{0.91(1)}$. Attempts to synthesize bulk samples of Ca_2AlPt_2 were successful, however, all syntheses of $CaAl_2Pt_2$ and Ca_2Al_3Pt led to the formation of multi-phase mixtures. Quantum-chemical calculations indicate that all three compounds are polar intermetallics with a designated charge transfer from the Ca/Al onto the Pt atoms while at the same time, distinct Al–Pt and homoatomic Al–Al/Pt–Pt bonding takes place. Therefore, the structures can be understood as $[Al_xPt_y]^{\delta-}$ polyanions with the Ca cations residing in cavities of the respective networks.

Author Contribution

All authors have accepted responsibility for the entire content of this submitted manuscript and approved the submission.

Acknowledgements

Instrumentation and technical assistance for this work were provided by the Service Center X-ray Diffraction, with financial support from Saarland University and German Research Foundation (project numbers INST 256/506-1 and INST 256/349-1). Funding was provided by the Deutsche Forschungsgemeinschaft DFG (JA 1891-10-1). Open Access funding enabled and organized by Projekt DEAL.

Conflict of Interest

The authors declare no conflicts of interest regarding this article.

Data Availability Statement

The data that supports the findings of this study are available from the corresponding author upon reasonable request.

Keywords: intermetallics · single-crystal · quantum-chemical calculations

[1] C. Benndorf, H. Eckert, O. Janka, *Acc. Chem. Res.* **2017**, *50*, 1459–1467.
[2] H. Eckert, R. Pöttgen, *Z. Anorg. Allg. Chem.* **2010**, *636*, 2232–2243.
[3] J. Emsley, *The Elements*, Clarendon Press, Oxford University Press, Oxford, New York, **1998**.
[4] F. Stegemann, T. Block, S. Klenner, Y. Zhang, B. P. T. Fokwa, A. Timmer, H. Mönig, C. Doerenkamp, H. Eckert, O. Janka, *Chem. Eur. J.* **2019**, *25*, 10735–10747.
[5] P. Villars, K. Cenzual, Pearson's Crystal Data: Crystal Structure Database for Inorganic Compounds, ASM International®, Materials Park, Ohio, USA **2023**.
[6] I. Doverbratt, S. Ponou, Y. Zhang, S. Lidin, G. J. Miller, *Chem. Mater.* **2015**, *27*, 304–315.
[7] F. Stegemann, C. Benndorf, R. S. Touzani, B. P. T. Fokwa, O. Janka, *J. Solid State Chem.* **2016**, *242*, 143–150.
[8] F. Stegemann, R. S. Touzani, O. Janka, *Dalton Trans.* **2019**, *48*, 14103–14114.
[9] F. Stegemann, T. Block, S. Klenner, Y. Zhang, B. P. T. Fokwa, C. Doerenkamp, H. Eckert, O. Janka, *Eur. J. Inorg. Chem.* **2021**, *2021*, 3832–3845.
[10] R.-D. Hoffmann, F. Stegemann, O. Janka, *Z. Kristallogr.* **2016**, *231*, 127–142.
[11] M. Radzieowski, F. Stegemann, R.-D. Hoffmann, O. Janka, *Z. Kristallogr.* **2017**, *232*, 675–687.
[12] P. Kenfack Tsobnang, D. Fotio, S. Ponou, C. Fon Abi, *Acta Crystallogr.* **2011**, *E67*, i55.
[13] F. Hulliger, *J. Alloys Compd.* **1993**, *196*, 225–228.
[14] F. Stegemann, Y. Zhang, B. P. T. Fokwa, O. Janka, *Dalton Trans.* **2020**, *49*, 6398–6406.
[15] S. Engel, E. C. J. Gießelmann, L. Schumacher, Y. Zhang, F. Müller, O. Janka, *Dalton Trans.* **2024**, in review.
[16] S. Engel, J. Bönnighausen, F. Stegemann, R. S. Touzani, O. Janka, *Z. Naturforsch.* **2022**, *77*, 367–379.
[17] S. Engel, O. Janka, *Z. Naturforsch.* **2024**, *79b*, accepted. DOI: 10.1515/znb-2024-0022.
[18] F. Stegemann, C. Benndorf, T. Bartsch, R. S. Touzani, M. Bartsch, H. Zacharias, B. P. T. Fokwa, H. Eckert, O. Janka, *Inorg. Chem.* **2015**, *54*, 10785–10793.
[19] M. Radzieowski, F. Stegemann, C. Doerenkamp, S. F. Matar, H. Eckert, C. Dosche, G. Wittstock, O. Janka, *Inorg. Chem.* **2019**, *58*, 7010–7025.
[20] T. Koizumi, F. Honda, Y. J. Sato, D. Li, D. Aoki, Y. Haga, J. Gouchi, S. Nagasaki, Y. Uwatoko, Y. Kaneko, Y. Ōnuki, *J. Phys. Soc. Jpn.* **2022**, *91*, 043704 (043705 pages).
[21] M. Radzieowski, F. Stegemann, O. Janka, *Eur. J. Inorg. Chem.* **2020**, *2020*, 1199–1210.
[22] M. Radzieowski, F. Stegemann, T. Block, J. Stahl, D. Johrendt, O. Janka, *J. Am. Chem. Soc.* **2018**, *140*, 8950–8957.
[23] R. Pöttgen, T. Gulden, A. Simon, *GIT Labor-Fachz.* **1999**, *43*, 133–136.
[24] R. Pöttgen, A. Lang, R.-D. Hoffmann, B. Künnen, G. Kotzyba, R. Müllmann, B. D. Mosel, C. Rosenhahn, *Z. Kristallogr.* **1999**, *214*, 143–150.
[25] Bruker AXS Inc., Topas, Version 5, Karlsruhe (Germany) **2014**.
[26] H. M. Rietveld, *Acta Crystallogr.* **1967**, *22*, 151–152.
[27] H. M. Rietveld, *J. Appl. Crystallogr.* **1969**, *2*, 65–71.
[28] Bruker AXS Inc., Saint+, Madison, WI (USA) **1999**.
[29] L. Palatinus, G. Chapuis, *J. Appl. Crystallogr.* **2007**, *40*, 786–790.
[30] V. Petříček, M. Dušek, L. Palatinus, Jana2006. The crystallographic computing system, Institute of Physics, Praha (Czech Republic) **2006**.
[31] V. Petříček, M. Dušek, L. Palatinus, *Z. Kristallogr.* **2014**, *229*, 345–352.
[32] V. Petříček, L. Palatinus, J. Plášil, M. Dušek, *Z. Kristallogr.* **2023**, *238*, 271–282.
[33] K. Brandenburg, Crystal Impact, Diamond, Bonn (Germany) **2022**.
[34] P. E. Blöchl, *Phys. Rev. B* **1994**, *50*, 17953–17979.
[35] G. Kresse, D. Joubert, *Phys. Rev. B* **1999**, *59*, 1758–1775.
[36] G. Kresse, J. Furthmüller, *Phys. Rev. B* **1996**, *54*, 11169–11186.
[37] G. Kresse, J. Furthmüller, *Comput. Mater. Sci.* **1996**, *6*, 15–50.
[38] R. F. W. Bader, *Chem. Rev.* **1991**, *91*, 893–928.
[39] K. Schubert, W. Burkhardt, P. Esslinger, E. Günzel, H. G. Meissner, W. Schütt, J. Wegst, M. Wilkens, *Naturwissenschaften* **1956**, *43*, 248–249.
[40] B. Eisenmann, N. May, W. Müller, H. Schäfer, *Z. Naturforsch.* **1972**, *27b*, 1155–1157.
[41] R. Pöttgen, *Z. Anorg. Allg. Chem.* **2014**, *640*, 869–891.
[42] D. Kußmann, R. Pöttgen, U. C. Rodewald, C. Rosenhahn, B. D. Mosel, G. Kotzyba, B. Künnen, *Z. Naturforsch.* **1999**, *54b*, 1155–1164.
[43] E. Parthé, L. M. Gelato, B. Chabot, M. Penzo, K. Cenzual, E. I. Gladyshevskii, *TYPIX–Standardized Data and Crystal Chemical Characterization of Inorganic Structure Types, in: Gmelin Handbook of Inorganic and Organometallic Chemistry*, Springer, Germany, Berlin, **1993**.
[44] D. Johrendt, H. Hosono, R.-D. Hoffmann, R. Pöttgen, *Z. Kristallogr.* **2011**, *226*, 435–446.
[45] C. Schwickert, R.-D. Hoffmann, F. Winter, R. Pöttgen, *Z. Kristallogr.* **2014**, *229*, 525–535.
[46] E. Zintl, A. Harder, W. Haucke, *Z. Phys. Chem. B* **1937**, *35*, 354–362.
[47] H. Nowotny, E. Wormnes, A. Mohrnheim, *Z. Metallkd.* **1940**, *32*, 39–42.
[48] E. A. Wood, V. B. Compton, *Acta Crystallogr.* **1958**, *11*, 429–433.
[49] E. C. J. Gießelmann, R. Pöttgen, O. Janka, *Z. Anorg. Allg. Chem.* **2023**, *649*, e202300109.
[50] O. Janka, R. Pöttgen, *Z. Naturforsch.* **2024**, *79b*, 63–70.
[51] F. Eustermann, F. Stegemann, S. Gausebeck, O. Janka, *Z. Naturforsch.* **2018**, *73b*, 819–830.
[52] T. Mishra, R.-D. Hoffmann, C. Schwickert, R. Pöttgen, *Z. Naturforsch.* **2011**, *66b*, 771–776.
[53] S. Seidel, O. Janka, C. Benndorf, B. Mausolf, F. Haarmann, H. Eckert, L. Heletta, R. Pöttgen, *Z. Naturforsch.* **2017**, *72b*, 289–303.
[54] E. C. J. Gießelmann, S. Engel, I. El Saudi, L. Schumacher, M. Radieowski, J. M. Gerdes, O. Janka, *Solids* **2023**, *4*, 160–180.

Manuscript received: June 3, 2024
Revised manuscript received: June 24, 2024
Accepted manuscript online: June 24, 2024

